Progress in Energy and Environment

Journal homepage: https://www.akademiabaru.com/submit/index.php/progee
Link to this article: https://doi.org/10.37934/progee.22.1.1328

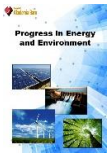

Volume 22 (2022) 13-28

Original Article

Synthesis and evaluation of Fe-doped zinc oxide photocatalyst for methylene blue and congo red removal

OPEN ACCESS

Cheah Tian Chee Kingsly[1], Jing Yao Sum[*,1,2]

[1] Department of Chemical and Petroleum Engineering, Faculty of Engineering, Technology and Built Environment, UCSI University, Kuala Lumpur, 56000, Malaysia
[2] UCSI-Cheras Low Carbon Innovation Hub Research Consortium, Kuala Lumpur Malaysia

Abstract

Zinc oxide is one of the most common photocatalyst utilized for the photocatalytic degradation of synthetic dyes aside from titanium dioxide. However, the application of ZnO in the treatment of wastewater containing synthetic dyes is limited due to the high energy band gap which allows ZnO to be efficient upon irradiation with ultraviolet radiation only. This study aims to reduce the energy band gap of ZnO through doping with Fe and to evaluate the photocatalytic degradation efficiency of the zinc oxide photocatalyst and its derivatives, specifically 0.25, 0.5, 2.5 and 5 mol% Fe(II)-doped ZnO, 0.25, 0.5, 2.5 and 5 mol% Fe(III)-doped ZnO and 2.5 mol% Fe(II)-Fe(III)-doped ZnO. The performance of the photocatalysts was evaluated based on the effect of solution pH, effect of photocatalyst loading and nature of dye. The synthesis of photocatalyst wwa done using sol-gel synthesis method, and photodegradation tests were carried out under visible light exposure for 60 minutes. The photocatalysts were characterized with SEM, FTIR, and UV-Vis spectroscopy. Based on the SEM images, it was found that the photocatalysts synthesized were agglomerated with irregular shape, having different grain sizes, and unequal size distribution. The doping of Fe to ZnO was successful according to the peak 513 cm^{-1} obtained from FTIR. The optical characterization results show that 2.5 mol% Fe(II)-Fe(III)-doped ZnO has the lowest band gap energy of 3.401 eV which was estimated using Tauc's plot. This further validated the degradation performance of the 2.5 mol% Fe(II)-Fe(III)-doped ZnO photocatalyst where it displayed the highest photocatalytic degradation efficiencies at all pH and photocatalyst loading. The highest degradation achieved using methylene blue was 94.21% and 32.97% for congo red using 300 mg/L photocatalyst loading at the optimum pH 10 and pH 4 respectively. Besides that, it was also found that the photocatalytic degradation efficiencies increased with increasing photocatalyst loading due to the increase in available active sites. The difference in photocatalytic degradation efficiencies of methylene blue and congo red at optimum pH and highest photocatalyst loading was due to the difference in point of zero charge and dissociation constant. In overall, the present study has proven that Fe-doped photocatalyst have the potential for the degradation of various synthetic dyes upon irradiation with visible light.

Article Info

Received 23 August 2022
Received in revised form 22 October 2022
Accepted 24 October 2022
Available online 29 November 2022

Keywords

Zinc oxide photocatalyst
Iron doping
Photocatalytic degradation
Band gap energy
Sol-gel method

[*] **Corresponding author** sumjy@ucsiuniversity.edu.my

1 Introduction

One of the major contributors to the worsening water pollution is the release of untreated industrial wastewater produced through various processes in various industries such as the agriculture industry, industrial manufacturing industry and oil and gas industry. The textile industry is an industry that mainly designs and manufactures clothing, fabrics and textiles which consumes a large volume of water during its manufacturing processes. Besides the high water consumption, the manufacturing processes also utilize a large amount of chemicals with the major chemical being synthetic dyes such as acid dyes, cationic dyes and azo dyes [1]. The high water consumption, coupled with large amounts of chemicals used, has led to the generation of a large amount of wastewater with a high concentration of synthetic dyes, making the textile industry the second largest contributor to global water pollution, accounting for approximately 20% of the global wastewater [2].

Two of the widely used synthetic dyes in the textile industry are methylene blue and congo red. Methylene blue, also known as methylthioninium chloride, is a type of cationic thiazine dye with a molecular formula of $C_{16}H_{18}ClN_3S$, while congo red, with a molecular formula of $C_{32}H_{22}N_6Na_2O_6S_2$, is a type of benzidine-based anionic diazo dye [3]. Both compounds are highly soluble in water which forms a stable solution under ambient conditions. In the textile industry, these compounds are mainly used to dye various textiles such as cotton, silk and wool. Other than the textile industry, methylene blue is also used in the pharmaceutical industry where it is commonly used as an antimalarial agent and antifungal agent for the treatment of diseases such as malaria and Alzheimer's, while congo red is also heavily used in histological studies and as an acid-base indicator due to its ability to turn red and blue in alkaline and acidic solution respectively [4,5]. Although methylene blue and congo red are significant to various industries especially the textile industry, these compounds are toxic and non-biodegradable which leads to various adverse health and environmental effects if left untreated in the wastewater [6]. For instance, when this compound is exposed to humans through skin, ingestion or inhalation, humans may experience various symptoms such as skin irritation, eye irritation, vomiting, nausea, gastrointestinal irritation and respiratory tract irritation. Exposure to methylene blue and congo red may also cause cancer in humans as these compounds are carcinogenic and mutagenic [7].

There are various treatment processes available to remove dyes from wastewater which could be categorized into physical methods, chemical methods and biological methods, and they differ from each other in terms of the effectiveness, removal efficiency, cost, complexity of the process and effect towards the environment [8]. Examples of these processes include adsorption, oxidation, precipitation, electrochemical destruction and one of the most promising technologies being applied and studied is the photocatalytic degradation method which is environmentally friendly and economical [9]. Photocatalytic degradation is a process of heterogeneous photocatalysis utilizing free radical mechanism whereby degradation of contaminants occurs in the presence of light and a semiconductor photocatalyst. Different semiconductor photocatalysts possess different band gap energy. Upon irradiation to light with band gap energy similar to or greater than that of the photocatalyst, the photocatalyst promotes the photocatalytic reaction, specifically the simultaneous oxidation and reduction reaction, where electron-hole pairs will be generated through the excitation of electrons of the semiconductor to the conduction band from the valence band [10]. These free charge carriers would then produce oxidizing agents when reacted with water or dissolved oxygen that degrades the contaminants.

Two of the most common semiconductor photocatalysts used for the photocatalytic degradation process are titanium dioxide, TiO_2, and zinc oxide, ZnO due to various advantages such as non-toxic and good photocatalytic efficiency. These photocatalysts have similar band gap energy with TiO_2 having a band gap energy of approximately 3.2 eV, and ZnO at approximately 3.37 eV [11,12]. Despite having similar band gap energies and advantages, ZnO has a slight edge over TiO_2 where the former is preferred for large-scale applications as it is more easily available, cheaper, and has relatively higher photocatalytic activity and efficiency when degrading certain compounds [13]. In several studies, it was reported that ZnO is an effective photocatalyst for the photocatalytic degradation of dyes. Zinc oxide photocatalyst can be prepared using several methods such as the sol-gel method, precipitation method, sonochemical method, microwave method and hydrothermal method. However, the use of ZnO as a photocatalyst comes with several disadvantages. One of the disadvantages of using ZnO as a

photocatalyst is the large band gap energy of 3.37 eV which indicates that photocatalysis using ZnO only occurs in the ultraviolet region of the solar spectrum. Since the solar spectrum only irradiates less than 5% ultraviolet radiation while 48% of the spectrum consists of visible light, photocatalysis using ZnO is inefficient due to the minimal photoexcitation of electrons from the valence band to the conduction band. Besides that, the photocatalysts used are hardly recovered from suspension after photocatalytic degradation and the recovery of ZnO from suspension is further complicated by its particle size as the particle size of ZnO being a nanocomposite is within the nano range [14]. Other than that, ZnO has shown poor photocatalytic activity and degradation efficiency which are largely due to the high recombination rate and large band gap energy [15]. To overcome these disadvantages, ZnO will have to undergo modifications such as doping with non-metals, doping with transition metals, and surface modifications.

Doping ZnO with transition metals is one of the highly researched and developed methods to improve the photocatalytic activity of ZnO where several dopants such as manganese, cobalt, and chromium were successfully doped into ZnO, resulting in the enhancement of the photocatalytic activity through the reduction of the band gap energy to the visible light region of the solar spectrum [16]. Since one of the major radiations of the solar spectrum is visible light, the reduction of band gap energy to visible light range allows for greater photocatalytic activity and effectiveness of photocatalyst in the photocatalytic degradation process as the photocatalyst will be able to absorb light of a larger range of wavelengths from the solar spectrum. Among all the transition metals, iron displayed unique characteristics when used as the dopant such as the reduction of the band gap energy depending on synthesis method, morphological change in ZnO, and promotes the separation of electron-hole pairs instead of recombination [17,18]. Furthermore, the photocatalyst can be doped with ferrites to synthesize a magnetic ferrite-based photocatalyst, allowing for the easy recovery of photocatalyst from suspension using magnetic separation techniques. Other than the enhancement of photocatalyst's properties, iron is also considered as a suitable dopant due to its abundance on Earth.

Despite the advantages of doping ZnO with iron, there are limited quantitative data available for the band gap energy of ZnO doped with various dosages of iron dopants, specifically Fe^{2+} and Fe^{3+}, and their photocatalytic degradation efficiencies. Reports on co-doping using mixture of Fe^{2+} and Fe^{3+} via sol-gel synthesis method were not available. Hence, this research aims to quantify the band gap energy of the newly synthesized photocatalyst and characterize using three characterization techniques. The dopants utilized were Fe(II), Fe(III) and mixture of Fe to reduce the band gap energy of ZnO. The photocatalytic activity and photocatalytic degradation efficiency of this newly-synthesized photocatalyst will be evaluated for the photocatalytic degradation of Methylene Blue and Congo Red based on the three factors, specifically the pH of solution, photocatalyst loading and nature of dyes.

2 Methodology and experimental setup

2.1 Materials

The zinc nitrate hexahydrate (Chemiz), iron (II) chloride tetrahydrate (Sigma-Aldrich), iron (III) chloride hexahydrate (Sigma-Aldrich), oxalic acid (Chemiz), sodium hydroxide (R&M Chemicals), 1 M hydrochloric acid (Chemiz), methylene blue and congo red used were AR grade.

2.2 Preparation of undoped zinc oxide

Zinc precursor solution of concentration 0.2 M was prepared by dissolving 5.9500 g of zinc nitrate hexahydrate in 100 mL of distilled water [19]. Then, 2.5214 g of oxalic acid dihydrate was dissolved in 100 mL of distilled water to produce 0.2 M oxalic acid [20]. This concentration of oxalic acid was chosen to maintain the molar ratio of oxalic acid to zinc precursor as 1:1 [21]. The solution was stirred at 350 rpm, and the solution was heated to 90°C using a holt plate magnetic stirrer [22]. Moving on, the 0.2 M oxalic acid solution was added to the zinc precursor solution to promote gel formation. The mixture was stirred for 3 hours to evaporate the solvents, and the gel-like mixture was allowed to cool down to room temperature. The gel was transferred to a petri dish and dried in a convective oven for 24 hours at 60°C. After drying for 24 hours, the precipitates were grounded using mortar and pestle. The dried and grounded precipitate was then calcined in a furnace at 750°C for 3 hours to obtain the photocatalyst [23].

2.3 Synthesis of iron(II)-doped zinc oxide and iron(III)-doped zinc oxide with varied concentration of dopant

Zinc precursor solution of concentration 0.2 M was prepared by dissolving 5.9500 g of zinc nitrate hexahydrate in 100 mL of distilled water [19]. Then, 0.0199 g of iron(II) chloride tetrahydrate was dissolved in 100 mL of distilled water to produce 0.001 M of iron(II) precursor solution which is equivalent to 0.25 mol% of 0.2 M zinc precursor solution. Moving on, 2.5214 g of oxalic acid dihydrate was dissolved in 100 mL of distilled water to produce 0.2 M oxalic acid [20]. This concentration of oxalic acid was chosen to maintain the molar ratio of oxalic acid to zinc precursor as 1:1 [21]. The solution was stirred at 350 rpm, and the solution was heated to 90°C using a hot plate magnetic stirrer. The iron(II) precursor solution was then added to the zinc precursor solution. The mixture was heated to 90°C, and the mixture was stirred for 15 minutes [22]. The 0.2 M oxalic acid solution was added to the mixture to promote gel formation. The mixture was stirred for 3 hours to evaporate the solvents, and the gel-like mixture was allowed to cool down to room temperature. The gel was transferred to a petri dish and dried in a convective oven for 24 hours at 60°C. After drying for 24 hours, the precipitates were grounded using mortar and pestle. The dried and grounded precipitate was then calcined in a furnace at 750°C for 3 hours to obtain the photocatalyst [23]. This methodology was repeated for other dosages of iron(II) ions dopant, specifically at 0.5 mol%, 2.5 mol% and 5 mol% [24,25]. The steps outlined above were repeated using iron(III) ions dopant by replacing the iron(II) chloride tetrahydrate with iron(III) chloride hexahydrate at the dosages 0.25 mol%, 0.5 mol%, 2.5 mol% and 5 mol%. The masses of iron(II) ions dopant and iron(III) ions dopant dissolved in 100 mL of distilled water for each specified dosage and added to the zinc precursor solution are tabulated in Table 1 and Table 2.

Table 1 Composition of Fe^{2+} ions dopants used for photocatalysts synthesis

Dosage (mol%)	Fe^{2+} Concentration (M)	Mass of $FeCl_2.4H_2O$ added (g)
0.25	0.001	0.0199
0.5	0.002	0.0398
2.5	0.01	0.1988
5	0.02	0.3976

Table 2 Composition of Fe^{3+} ions dopants used for photocatalysts synthesis.

Dosage (mol%)	Fe^{3+} Concentration (M)	Mass of $FeCl_3.6H_2O$ added (g)
0.25	0.001	0.0270
0.5	0.002	0.0541
2.5	0.01	0.2703
5	0.02	0.5406

2.4 Preparation of mixed iron(II)-iron(III)-doped zinc oxide

The procedures utilized for the preparation of magnetic iron(II)-iron(III)-doped zinc oxide were similar to the procedures outlined in Section 2.2 for the preparation of iron-doped zinc oxide. After the preparation of zinc precursor solution, the iron(II)-iron(III) precursor solution was prepared by first dissolving 0.0663 g of iron(II) chloride tetrahydrate in 100 mL of distilled water to produce 0.0033 M of iron(II) precursor solution. Then, 0.1802 g of iron(III) chloride hexahydrate was dissolved in 100 mL of distilled water to produce 0.0067 M of iron(III) precursor solution. The molar ratio of Fe(III):Fe(II) was 2:1 [26]. The iron(III) precursor solution was placed on the hot plate magnetic stirrer. The solution was stirred at 350 rpm, and the solution was heated to 90°C. The iron(II) precursor solution was then added to the iron(III) precursor solution. The mixture was then heated to 90°C, and the mixture was stirred for 15 minutes. The subsequent synthesis steps performed were similar to the steps in Section 2.2 until the end of calcination.

2.5 Characterization of photocatalyst

The synthesized photocatalysts were characterized using scanning electron microscope (SEM), Fourier Transform Infrared (FTIR) Spectroscopy, and UV-Vis spectroscopy. The SEM was utilized to study the morphologies of the newly synthesized photocatalyst. The morphology of the photocatalysts was characterized using the tabletop SEM (TM3000, Hitachi) which was operated with the accelerating voltage in 15 kV mode. First, the photocatalyst was ground into fine powder and spread evenly on carbon tape. Then, the micrograph SEM was performed using two magnification settings, specifically x1.0k and x3.0k magnification. FTIR (VERTEX 70v, Bruker) was utilized to evaluate the chemical properties of the newly synthesized photocatalysts, specifically the chemical bonds and functional groups present. The IR spectra of the photocatalysts were obtained in the wavelength range of 550 cm^{-1} to 4000 cm^{-1}, with resolution of 4 cm^{-1}. The band gap energies of four synthesized photocatalysts, specifically undoped ZnO, 5 mol% Fe(II)-doped ZnO, 5 mol% Fe(III)-doped ZnO, and 5 mol% Fe(II)-Fe(III)-doped ZnO, were quantified using Tauc plot. The absorption spectra for each of the photocatalyst was obtained using UV-Vis spectroscopy. The concentrations of methylene blue and congo red used for the analysis were 10 ppm, 20 ppm, 30 ppm, 40 ppm, and 50 ppm. The characteristic absorption peaks for all concentrations of methylene blue and congo red were localized at 600 nm and 498 nm respectively.. These wavelengths were utilized during the determination of absorbance for each sample taken during the photodegradation test involving methylene blue and congo red as model solutes.

The Tauc plot can be expressed as the following Eq. (1), Eq. (2), and Eq. (3) [27].

$$(\alpha \cdot h\nu)^{1/\gamma} = B(h\nu - E_g) \tag{1}$$

$$I = I_0 e^{-\alpha t} \text{ and } A = \log(I_o / I) \tag{2}$$

$$\alpha = 2.303\left(\frac{A}{t}\right) \tag{3}$$

After the calculation of hv and $(\alpha h\nu)^2$, a graph of $(\alpha h\nu)^2$ versus $h\nu$ was plotted for each photocatalyst to estimate the band gap energy. This graph is known as the Tauc plot. The region of linear increase of $h\nu$ and $(\alpha h\nu)^2$ indicates the energy band gap characteristic of the photocatalyst. The band gap energies of each photocatalyst were obtained by extrapolating the linear line found to the *x*-axis and the estimated band gap energies were the *x*-intercept [28].

2.6 Performance evaluation

For the evaluation of the performance of the synthesized photocatalysts during the photocatalytic degradation, the effect of nature of dye, solution pH, and photocatalyst loading on the photocatalytic degradation efficiency of methylene blue and congo red were evaluated. The photocatalytic degradation using the undoped zinc oxide photocatalyst and the three magnetic iron-doped zinc oxide photocatalysts were conducted under visible light irradiated using quartet of 150W equivalent E27 15W LED bulbs. The photocatalytic degradation efficiency can be calculated using Eq. (4),

$$\eta\% = \frac{C_0 - C_t}{C_0} \times 100\% \tag{4}$$

where,

η = Photocatalytic degradation efficiency of photocatalyst, %
C_0 = Initial concentration of dye at time 0, ppm
C_t = Concentration of dye at time *t*, ppm

To begin the experiment, 95 mL of distilled water was measured and transferred to a transparent glass. Then, 5 mL of 1000 ppm methylene blue was pipetted and added into the glass, forming 50 ppm methylene blue solution. The transparent glass was then placed in to the experimental setup container, and 3 mL of solution was taken from the glass and the initial methylene blue concentration was determined using UV-Vis. The container was closed to avoid interference from the surrounding.. After 30 minutes, another 3 mL of solution was taken from the glass and the changes in methylene blue concentration was recorded. The LED light bulbs were then switched on to expose the 50 ppm methylene blue under visible light. Samples of 3 mL volume were taken at intervals of 10 minutes for 60 minutes The absorbance of the eight samples was measured using UV-Vis spectrophotometer. The

concentrations of each sample were obtained from the calibration curves plotted and the changes of methylene blue (without the presence of photocatalyst) under visible light irradiation was monitored. The steps outlined were repeated for 50 ppm congo red.

To begin the experiment for pH variation, 100 mL of distilled water was prepared in a 250 mL beaker. The initial pH of distilled water was measured. The beaker was then placed on a magnetic stirrer, and the distilled water was stirred at 400 rpm. The pH of the distilled wated were adjusted to pH 4 by the addition of 0.1 M hydrochloric acid to lower the pH and 0.1 M sodium hydroxide solution to increase the pH. After the adjustment of pH to pH 4, 95 mL of the pH 4 water was measured and added in a transparent glass. Then, 0.01 g of undoped zinc oxide was added to the glass containing the pH 4 water. The heterogeneous mixture was ultrasonicated at 75% amplitude and one cycle for 90 seconds to improve the dispersion of photocatalyst [29]. Then, 5 mL of 1000 ppm methylene blue was pipetted and added to the glass. The transparent glass was then placed in to the experimental setup container, and 3 mL sample was taken from the glass. The container was closed, and the mixture of photocatalyst and methylene blue was stirred for 30 minutes under dark condition to achieve adsorption-desorption equilibrium [30]. The sample was centrifuged at 3500 rpm for 5 minutes, and 2 mL of the supernatant was taken for determining the concentration of methylene blue. After 30 minutes, another 3 mL of solution was removed from the glass. The LED light bulbs were then switched on to expose the mixture to visible light. The second sample was again centrifuged at 3500 rpm for 5 minutes, and 2 mL of the supernatant was taken for characterization. Samples of 3 mL were taken at intervals of 10 minutes for 60 minutes, centrifuged at 3500rpm for 5 minutes and 2 mL of the supernatant was taken for characterization [31]. The concentrations of methylene blue in the collected samples were measured using UV-Vis spectrophotometer. Hence, the percentage of photodegradation was calculated. The steps outlined were repeated at pH 7 and pH 10 by adjusting the pH of the solution using 0.1 M hydrochloric acid to reduce the pH and 0.1 M sodium hydroxide to increase the pH. The experiment was repeated using the 0.5 mol% iron(II)-doped zinc oxide photocatalyst and 0.25 mol% iron(III)-doped zinc oxide photocatalysts to replace the undoped zinc oxide.

For the experiment varying photocatalyst loading, the procedures performed were similar to the procedures above. The experiment was conducted using the newly synthesized undoped zinc oxide, iron(II)-doped zinc oxide photocatalysts at optimum Fe(II) dosage and iron(III)-doped zinc oxide photocatalysts at optimum Fe(III) dosage. The pH utilized was the optimum pH determined. The photocatalyst loading was varied to 200 mg/L and 300 mg/L.

3 Results and Discussion

3.1 Characterization of functional groups

The FTIR spectrum of four photocatalysts is illustrated in Fig. 2, specifically the FTIR spectrum for undoped ZnO, 2.5 mol% iron(II)-doped ZnO, 2.5 mol% iron(III)-doped ZnO and 2.5 mol% iron(II)-iron(III)-doped ZnO. The infrared absorption spectra of the photocatalysts were observed in the wavenumber range of 350-4000 cm^{-1}. The main absorption bands of the photocatalysts were observed at 404 cm^{-1}, 513 cm^{-1} and 1760 cm^{-1} with a slight difference in the intensities of each peak. The weak peak at 1760 cm^{-1} is attributed to the C=O stretching group of carboxylic acid. This peak C=O hints the presence of unremoved oxalic acid which is used as the gelling agent. Moving on, the band at 513 cm^{-1} is attributed to the Fe-O stretching as the peak of the doped photocatalysts became stronger in comparison to the undoped ZnO, thus indicating the successful doping of iron dopants. The band at 404 cm^{-1} may be attributed to the Zn-O bond stretching or vibration [8].

According to Fig. 1, there were no significant changes to the spectra between undoped ZnO and doped ZnO for the three different dopants. The main difference observed based on the spectra was the peak observed at the band 513 cm^{-1} where the peak could be attributed to the Fe-O stretching. The shortest peak at this band was observed in undoped ZnO followed by the mixed iron(II)-iron(III)-doped ZnO, 2.5 mol% iron(III)-doped ZnO, and the strongest peak in 2.5 mol% iron(II)-doped ZnO. The increasing peak intensity attributed to the Fe-O stretching indicates the successful incorporation of iron as dopant in the zinc oxide photocatalyst. The strongest peak found in 2.5 mol% iron(II)-doped ZnO suggested that the photocatalyst has the highest amount of dopant doped to the ZnO. Aside from the

peak intensity, there was a slight redshift for all the doped photocatalysts as compared with the pristine ZnO.

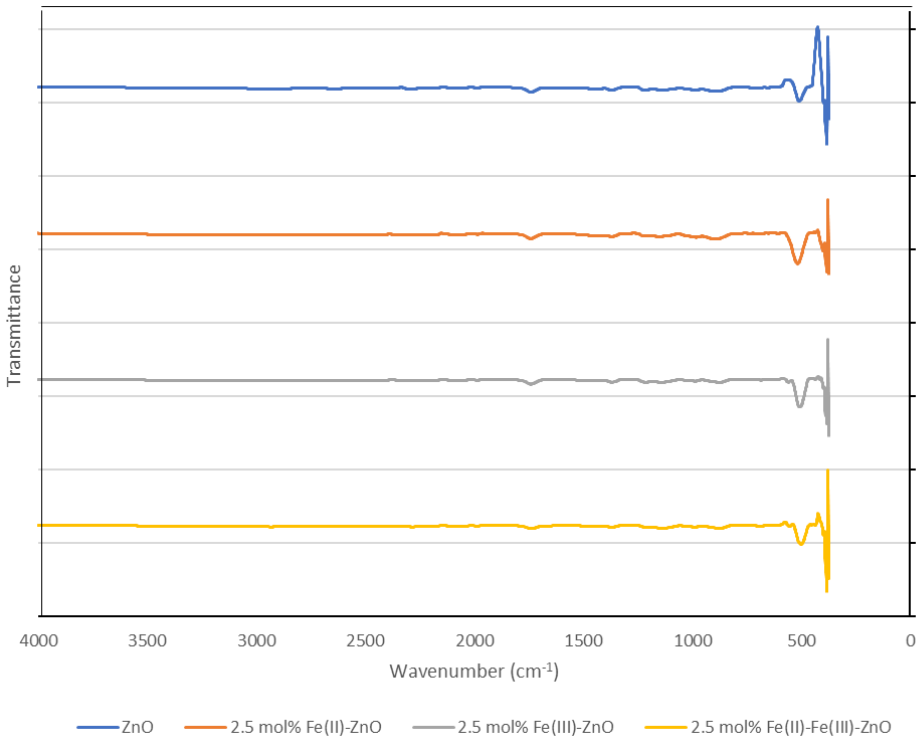

Fig. 1 FTIR spectra of synthesized photocatalysts.

3.2 SEM analysis of zinc oxide

According to Fig. 2, the surface morphology of the undoped zinc oxide synthesized using sol-gel synthesis method was amorphous where the nanoparticles are agglomerated with irregular shapes. The agglomerates of the nanoparticles were of unequal size distribution with different grain sizes which are evident in the SEM images of the undoped zinc oxide photocatalyst. A similar result was reported by another study synthesizing ZnO nanoparticles using the same synthesis method [32]. In a study reported by Lu et al [33], the powdered nanoparticles were pretreated to prevent the agglomeration of the nanoparticles, thus producing SEM micrographs that displayed the discrete shapes and sizes of the nanoparticles.

3.3 SEM analysis of iron(II)-doped zinc oxide and iron(III)-doped zinc oxide

The surface morphology analyses were performed for the four iron(II)-doped zinc oxide synthesized with different dosages of Fe^{2+} ions and the four iron(III)-doped zinc oxide synthesized with different dosages of Fe^{3+} ions. The SEM images were compared with the SEM images of undoped zinc oxide as shown in Fig. 3 and Fig. 4. It was found that the morphologies of the iron(II)-doped zinc oxide photocatalyst and iron(III)-doped zinc oxide photocatalyst had the same morphology with the undoped zinc oxide, where the nanoparticles are agglomerated with irregular shape, having different grain sizes, and unequal size distribution. At the doping dosage of 2.5 mol%, it can be observed that the sizes of the particles were decreasing with increasing dosage, thus indicating the formation of photocatalysts. The morphologies of the 2.5 mol% and 5 mol% Fe(II)-ZnO and Fe(III)-ZnO were flaky in comparison to ZnO and photocatalysts of lower dosage.

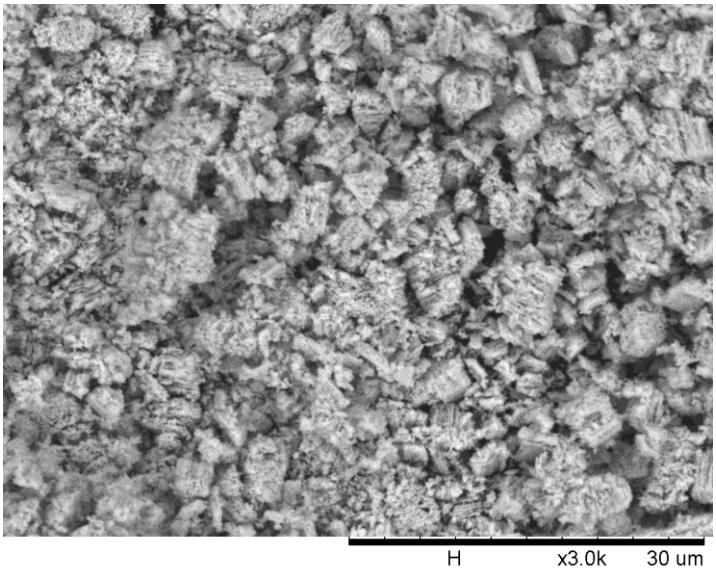

Fig. 2 SEM micrograph of undoped zinc oxide at x3.0k magnification.

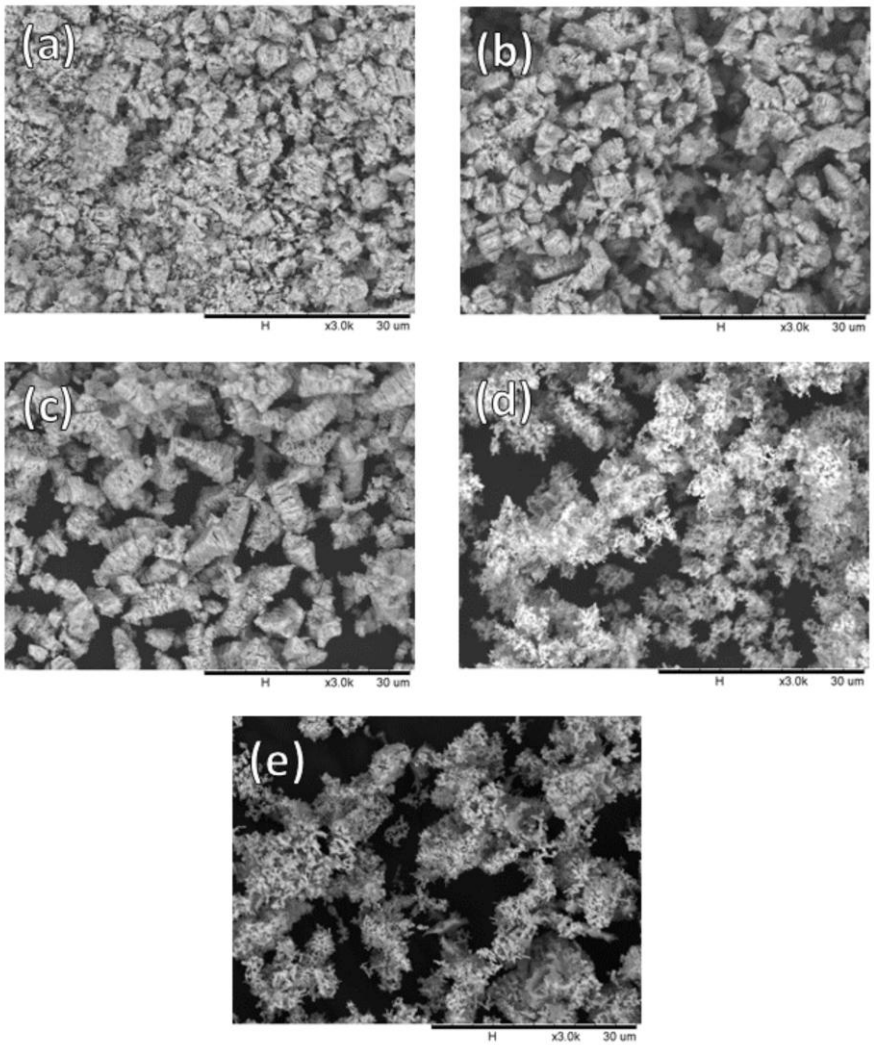

Fig. 3 SEM images of (a) undoped ZnO, (b) 0.25 mol% Fe(II)-doped ZnO, (c) 0.5 mol% Fe(II)-doped ZnO, (d) 2.5 mol% Fe(II)-doped ZnO and (e) 5 mol% Fe(II)-doped ZnO at x3.0k magnification.

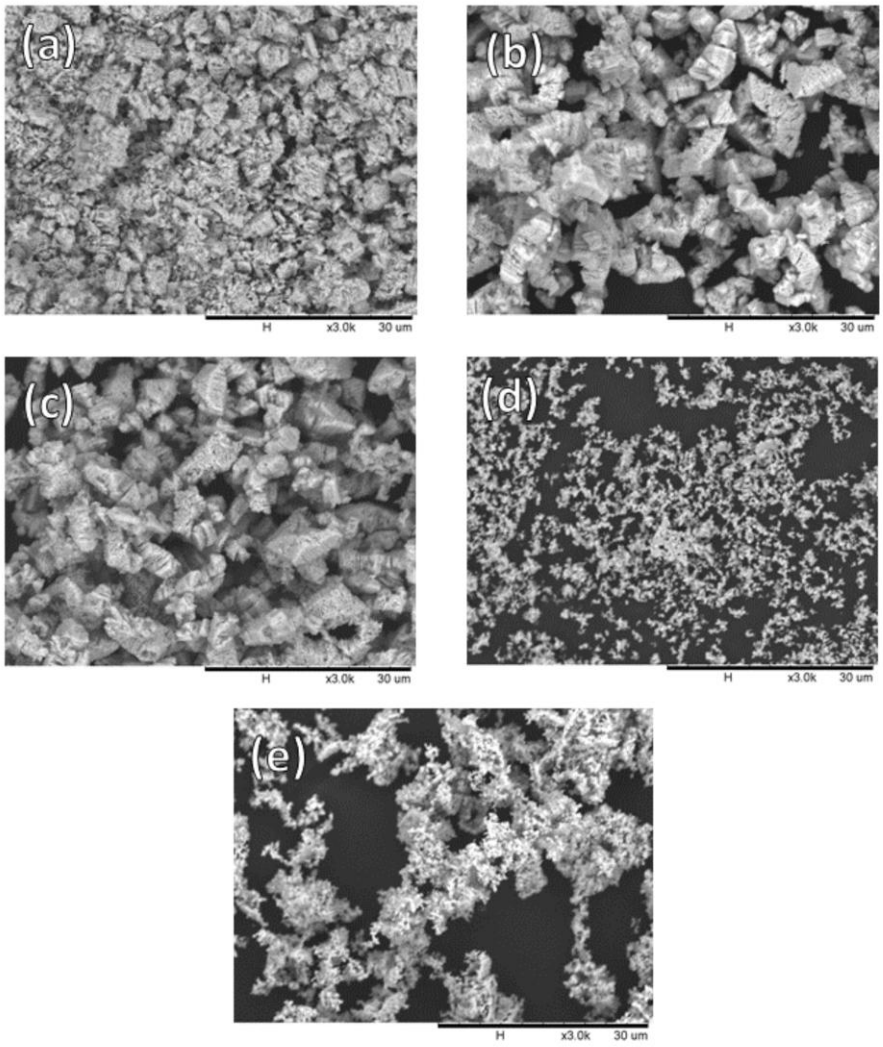

Fig. 4 SEM images of (a) undoped ZnO, (b) 0.25 mol% Fe(III)-doped ZnO, (c) 0.5 mol% Fe(III)-doped ZnO, (d) 2.5 mol% Fe(III)-doped ZnO and (e) 5 mol% Fe(III)-doped ZnO at x3.0k magnification.

3.4 Energy band gap quantification

The energy band gap of four photocatalysts was determined using Tauc plot. The energy band gap of the four photocatalysts quantified were undoped ZnO, 2.5 mol% iron(II)-doped ZnO, 2.5 mol% iron(III)-doped ZnO and 2.5 mol% iron(II)-iron(III)-doped ZnO. The Tauc plot for each photocatalyst is displayed in Fig. 5, and the summary of the energy band gaps of each photocatalyst was tabulated in Table 3.

According to the band gap energies tabulated in Table 3, it was proved that the 2.5 mol% Fe(II)-Fe(III)-doped ZnO had the lowest band gap energy among the other photocatalyst which justified the photocatalytic degradation efficiencies obtained in the experiments where 2.5 mol% Fe(II)-Fe(III)-doped ZnO achieved the highest photocatalytic degradation efficiencies at all pH and photocatalyst loading. The 2.5 mol% Fe(II)-doped ZnO had the second lowest band gap energy of 3.404 eV, followed by 2.5 mol% Fe(III)-doped ZnO and lastly undoped ZnO. This trend of band gap energies further clarified and validated the results obtained in the experiments conducted.

The band gap energy of Fe-doped ZnO displayed a red shift as the band gap energies of all doped photocatalysts were lower than the band gap energy of undoped ZnO with a value of 3.408 eV. The reduction in energy band gap of doped ZnO was largely contributed by the valence electrons of Fe in which the valence of Fe is larger than the valence of Zn. With larger valence electrons, the Fe acted as

an electron donor which eased the transition of electron from the valence band to the conduction band, thus reducing the energy required to excite electrons from valence band to conduction band [34].

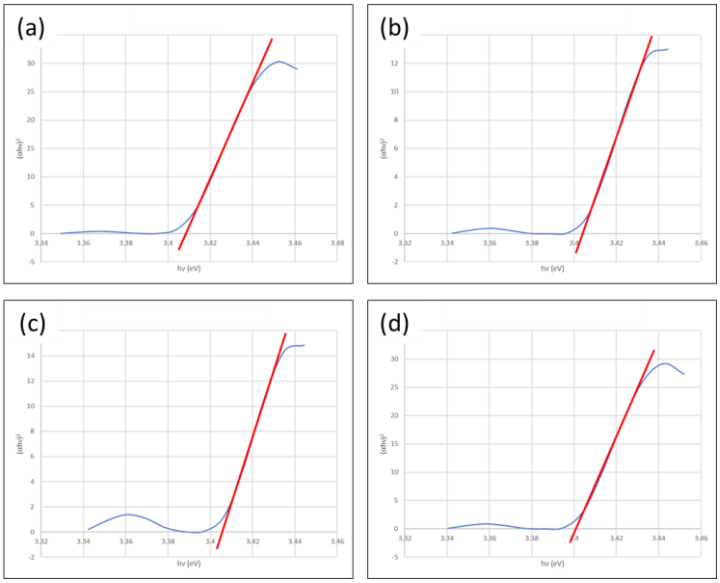

Fig. 5 Tauc plot for (a) undoped zinc oxide, (b) 2.5 mol% Fe(II)-doped ZnO, (c) 2.5 mol% Fe(III)-doped ZnO and (d) 2.5 mol% Fe(II)-Fe(III)-doped ZnO.

Table 3 Band gap energies of photocatalysts determined from Tauc plot.

Photocatalyst	Band gap energies (eV)
Undoped ZnO	3.408
2.5 mol% Fe(II)-doped ZnO	3.404
2.5 mol% Fe(III)-doped ZnO	3.406
2.5 mol% Fe(II)-Fe(III)-doped ZnO	3.401

3.5 Photocatalytic degradation efficiency

3.5.1 Effect of pH

The effect of solution pH, specifically at pH 4, pH 7, and pH 10, with the undoped ZnO and the two derivatives, 0.25 mol% Fe(II)-doped ZnO and 0.25 mol% Fe(III)-doped ZnO, were evaluated to determine the optimum solution pH for photocatalytic degradation of methylene blue and the optimum dosages of dopant. The experiment began with the determination of optimum solution pH for the three photocatalysts using methylene blue as model solute. The summary of photocatalytic degradation efficiencies for each photocatalyst at each pH is tabulated in Table 4.

Table 4 Photocatalytic degradation efficiencies of photocatalysts at different solution pH using 100 mg/L photocatalyst loading in methylene blue solution.

Photocatalyst	Photocatalytic Degradation Efficiency (%)		
	pH 4	pH 7	pH 10
Undoped ZnO	24.53	38.68	88.53
0.25 mol% Fe(II)-doped ZnO	25.10	41.20	90.63
0.25 mol% Fe(III)-doped ZnO	20.34	34.76	90.45

From Table 4, it was proved that all three photocatalysts were inefficient at acidic and neutral pH, while the highest photocatalytic degradation efficiencies were obtained at pH 10 for all three photocatalysts. The three photocatalysts displayed similar trends in photocatalytic degradation

efficiencies at different pH, where the lowest efficiencies were obtained at pH 4, followed by pH 7, and the highest at pH 10. Hence, it can be concluded that the optimum pH for methylene blue degradation is pH 10 for all three photocatalyst. In comparison between the three photocatalysts at optimum pH, 0.25 mol% Fe(II)-doped ZnO displayed the highest efficiency at 90.63% followed by 0.25 mol% Fe(III)-doped ZnO at 90.45% and lastly, undoped ZnO at 88.53%, indicating that doping of ZnO produced photocatalysts with lower band gap energy than undoped ZnO.

In general, the variation of solution pH will cause the variation of surface charges of the photocatalysts which will subsequently cause the shifting of potential of the photocatalytic reaction [35,36]. Under acidic condition at pH 4 or basic condition at pH 10, protonation or deprotonation will occur respectively on the surface of the photocatalysts [36]. At pH 4, the surface of photocatalysts became protonated due to the increase in the concentration of hydrogen ions, thus causing the surface of the photocatalysts to be positively charged, whereas the surface of photocatalysts became deprotonated at pH 10 due to the increase in the concentration of hydroxide ions which caused the surface of the photocatalysts to be negatively charged. Methylene blue is a type of cationic dye, indicating that methylene blue is a positively charged dye. In addition to the changes of surface charges of photocatalyst, changes in pH will enhance the charge of the molecules through changes in the electrostatic forces of attraction where positively charged dye will be enhanced due to the deprotonation of photocatalyst and vice versa [37]. At pH 10, the surface charges of photocatalysts were negative which would promote the adsorption of methylene blue molecules on the surface of the photocatalyst due to the electrostatic attraction forces between opposite charges, whereas the adsorption of methylene blue molecules on the surface of the positively charged photocatalyst at pH 4 was opposed due to the electrostatic repulsive forces between similar charges [3]. Other than that, at higher pH, more hydroxide ions are available for the formation of hydroxyl radicals upon reaction with holes, thus promoting the degradation of positive methylene blue dye as more hydroxyl radicals were available to attack and degrade the methylene blue molecules [35].

For the determination of optimum dosages of dopant, photodegradation tests for the doped ZnO at different dosages of dopants using pH 10 were conducted, and the summary of photocatalytic degradation efficiencies for each photocatalyst at different dosages is tabulated in Table 5.

Table 5 Photocatalytic degradation efficiencies of photocatalysts at pH 10 using 100 mg/L photocatalyst loading in methylene blue solution.

Photocatalyst	Photocatalytic Degradation Efficiency (%)			
	0.25 mol%	0.5 mol%	2.5 mol%	5 mol%
Fe(II)-doped ZnO	90.63	91.56	92.68	92.42
Fe(III)-doped ZnO	90.45	91.49	91.77	90.17

From Table 5, it was proved that the optimum dosages of dopant for both Fe-doped ZnO photocatalysts were 5 mol% as the highest photocatalytic degradation efficiencies were obtained at this dosage. The trend of photocatalytic degradation efficiencies for both the Fe(II)-doped ZnO and Fe(III)-doped ZnO was similar as it was observed that the degradation efficiencies increased from the lowest dosage of 0.25 mol% to 2.5 mol% before decreasing at 5 mol% of dopants. Hence, it can be concluded that the optimum dosage of dopant is 2.5 mol% and this dosage percentage was utilized for the synthesis of Fe(II)-Fe(III)-doped ZnO.

3.5.2 Effect of photocatalyst loading

The effect of photocatalyst loading, specifically at 100 mg/L, 200 mg/L and 300 mg/L, with the undoped ZnO and two derivatives at optimum dosage, 2.5 mol% Fe(II)-doped ZnO and 2.5 mol% Fe(III)-doped ZnO, on the photocatalytic degradation of methylene blue were evaluated to determine the changes towards photocatalytic degradation efficiencies by varying the amount of photocatalyst added in each photodegradation tests. The solution pH utilized was fixed at pH 10, the optimum pH determined as reported in Section 3.5.1. The summary of photocatalytic degradation efficiencies for each photocatalyst using different photocatalyst loading at pH 10 is tabulated in Table 6.

Table 6 Photocatalytic degradation efficiencies of photocatalysts at pH 10 using different photocatalyst loading in methylene blue solution.

Photocatalyst	Photocatalytic Degradation Efficiency (%)		
	100 mg/L	200 mg/L	300 mg/L
Undoped ZnO	88.53	90.69	91.51
2.5 mol% Fe(II)-doped ZnO	92.68	92.74	93.29
2.5 mol% Fe(III)-doped ZnO	91.77	92.34	92.72

From Table 6, it was proved that there were increments in the photocatalytic degradation efficiencies for all three tested photocatalysts when the dosage of photocatalyst was increased. The three photocatalysts displayed similar trends in photocatalytic degradation efficiencies using different amount of photocatalysts, where the photocatalytic degradation efficiencies increase with increasing photocatalyst loading. Similarly, the ZnO photocatalyst doped with Fe(II) ions displayed the highest photocatalytic degradation efficiency at 93.29% when the loading of 300 mg/L was utilized. At another photocatalyst loading, 2.5 mol% Fe(II)-doped ZnO also had the highest photocatalytic degradation efficiency in comparison with the other two photocatalysts using the same amount of photocatalyst. In comparison between the three photocatalysts, 2.5 mol% Fe(II)-doped ZnO displayed the highest photocatalytic degradation efficiency at all photocatalyst loading, followed by 2.5 mol% Fe(II)-doped ZnO, and lastly, undoped ZnO with the lowest efficiencies across all photocatalyst loadings. These results further justified the reduction of band gap energy of ZnO when doped with Fe dopants and indicate the success of doping.

In general, photocatalytic degradation efficiency will increase with the increase in the amount of photocatalysts added to the dye solution. Based on the experiments conducted in this research, the increase in photocatalytic degradation efficiency can be attributed to the increase in the number of available active sites due to the increase in the amount of photocatalyst. Since the number of available active sites increased, more methylene blue molecules were adsorbed on the surface of photocatalysts and more hydroxyl radicals were formed for degradation of methylene blue molecules which resulted in greater activity of photocatalytic degradation, thus higher photocatalytic degradation efficiencies. According to several studies, increasing the photocatalyst loading could cause the reduction of photocatalytic degradation efficiency [19,35,36]. This phenomenon could be caused by various reasons such as the masking effect where photocatalysts could block methylene blue molecules from being adsorbed onto the surface of photocatalyst, agglomeration of photocatalysts which reduces the photoexcitation of electrons, or increase in the turbidity of solution which prevents UV and visible light radiation from reaching the photocatalysts [19,35,36]. However, this trend was not observed in this research as the maximum photocatalyst loading of 300 mg/L used in this research was not high enough to cause the reduction in efficiencies.

3.5.3 Effect of nature of dye

The effect of nature of dye was evaluated using two different types of dyes with different charges, specifically methylene blue as cationic dye which is positively charged and congo red as anionic dye which is negatively charged. The photocatalyst used for this set of experiments was the 2.5 mol% Fe(II)-Fe(III)-doped ZnO photocatalyst. The experiment began with the determination of optimum pH using both model solutes, followed by the determination of the effect of photocatalyst loading at the respective model solutes' optimum pH. The summary of photocatalytic degradation efficiencies for each model solutes at different pH and photocatalyst loading is tabulated in Table 7 and Table 8.

According to the results tabulated in Table 7, it was proved that the optimum pH for the degradation of methylene blue is pH 10 while the optimum pH for the degradation of congo red is pH 4. In terms of methylene blue, the highest photocatalytic degradation efficiencies were obtained at pH 10 at 94.21% and the lowest at 27.10% when using pH 4. The photodegradation tests of methylene blue displayed a trend, where the photocatalytic degradation efficiency increases with the increase of pH. As for congo red, the highest photocatalytic degradation efficiencies were obtained at pH 4 at 4.55% and the lowest at 3.72% when using pH 10. The photodegradation tests of congo red displayed an opposite trend in

comparison to methylene blue, where the photocatalytic degradation efficiency increases with the decrease in pH.

Table 7 Photocatalytic degradation efficiencies of 2.5 mol% Fe(II)-Fe(III)-doped ZnO photocatalyst using different model solutes at 100 mg/L photocatalyst loading.

Model solute	Photocatalytic Degradation Efficiency (%)		
	pH 4	pH 7	pH 10
Methylene blue	27.10	46.62	93.21
Congo red	4.55	4.33	3.72

Table 8 Photocatalytic degradation efficiencies of 2.5 mol% Fe(II)-Fe(III)-doped ZnO photocatalyst at optimum pH using different photocatalyst loading.

Model solute	Optimum pH	Photocatalytic Degradation Efficiency (%)		
		100 mg/L	200 mg/L	300 mg/L
Methylene blue	10	93.21	94.00	94.21
Congo red	4	4.55	19.41	32.97

The difference between the optimum pH of congo red in comparison with the optimum pH of methylene blue can be explained using the similar concept for the effect of solution pH. At pH 4, the surface of photocatalysts became protonated due to the increase in the concentration of hydrogen ions, thus causing the surface of the photocatalysts to be positively charged, whereas the surface of photocatalysts became deprotonated at pH 10 due to the increase in the concentration of hydroxide ions which caused the surface of the photocatalysts to be negatively charged. Congo red is a type of anionic dye, indicating that congo red is a negatively charged dye. At pH 4, the surface charges of photocatalysts were positive due to protonation which would promote the adsorption of congo red molecules on the surface of the photocatalyst due to the electrostatic attraction forces between opposite charges, whereas the adsorption of congo red molecules on the surface of the negatively charged photocatalyst at pH 10 was opposed due to the electrostatic repulsive forces between similar charges.

From Table 8, it was proved that increasing photocatalyst loading resulted in the increase of photocatalytic degradation efficiencies for both model solutes. The highest degradation when using methylene blue as the model solute in pH 10 solution was at 300 mg/L of photocatalyst with an efficiency of 94.21%, whereas the highest degradation when using congo red as the model solute in pH 4 solution was at 300 mg/L of photocatalyst with an efficiency of 32.97%. The increase in photocatalytic degradation efficiencies for both model solutes can be justified using similar justifications stated in Section 3.5.2, where an increase in amount of photocatalysts added increased the number of active sites, thus promoting more adsorption of dye molecules on the surface of the photocatalysts, resulting in the increase in activity of photocatalytic degradation.

However, based on both Table 7 and Table 8, it was proved that the photocatalytic degradation efficiencies when using congo red as model solute were significantly lower than the efficiencies obtained using methylene blue as model solute despite using the optimum solution pH. Adsorption of dye molecules on the surface of photocatalyst involves two attraction forces, namely the electrostatic forces of attraction and hydrogen bonding [38]. The difference can be justified based on the point of zero charge. Point of zero charge is the pH in which there are no net charges on the surface of the photocatalyst. Based on the results obtained for congo red, the optimum pH identified, pH 4, was still very close to the point of zero charge, thus limiting the photocatalytic degradation of congo red.
According to a study, the point of zero charge of congo red degradation is pH 6.2 and the optimum pH was found to be pH 3 [39]. In a follow up photodegradation tests conducted for this research, it was found that significant photocatalytic degradation occurred at pH 2. Besides point of zero charge, the difference was caused by the difference in dissociation constant of methylene blue and congo red. The dissociation constant of methylene blue is 3.8 and congo red has a dissociation constant of 4.5 [40,41]. Protonation occurred to the dye molecules when the solution pH utilized was below the dissociation

constants, and the dye molecules remained unchanged for pH above the dissociation constants. Therefore, this justified the degradation efficiency of methylene blue. For the case of congo red, the adsorption onto the photocatalyst's surface was more dependent on the isoelectric point. The isoelectric point of congo red is 3. At pH higher than 3, the congo red molecule will remain negatively charged, thus allowing electrostatic attraction to occur during the adsorption onto the surface of photocatalyst [42].

4 Conclusion

In this research, photocatalysts were successfully synthesized using sol-gel synthesis method, specifically, undoped ZnO, 0.25, 0.5, 2.5 and 5 mol% Fe(II)-doped ZnO, 0.25, 0.5, 2.5 and 5 mol% Fe(III)-doped ZnO and 2.5 mol% Fe(II)-Fe(III)-doped ZnO. The performance of the synthesized photocatalysts were evaluated based on the effect of solution pH, photocatalyst loading and nature of dye were studied. The synthesized photocatalysts were characterized with SEM, FTIR and UV-Vis spectroscopy.

Through this study, it was found that 2.5 mol% Fe(II)-Fe(III)-doped ZnO had the highest photocatalytic degradation pH at all solution pH and photocatalyst loading followed by 2.5 mol% Fe(II)- doped ZnO, 2.5 mol% Fe(III)-doped ZnO and undoped ZnO. The solution pH investigated were pH 4, pH 7 and pH10, while the photocatalyst loading investigated were 100 mg/L, 200 mg/L and 300 mg/L. The highest photocatalytic degradation achieved was 94.21% during the degradation of methylene blue and 32.97% for congo red using 300 mg/L of 2.5 mol% Fe(II)-Fe(III)-doped ZnO at pH 10 and pH 4 respectively. The difference in optimum pH was due to the surface charges on the surface of photocatalyst and the charge of the cationic and anionic dye. It was also found that the improvement in photocatalytic degradation efficiency at high photocatalyst loading was due to the increase in number of available active sites for the adsorption of synthetic dye molecules.

Lastly, band gap energy of the undoped ZnO and 2.5 mol% iron-doped photocatalysts were quantified. It was found that the 2.5 mol% iron(II)-iron(III)-doped ZnO had the lowest band gap energy of 3.401 eV, followed by 2.5 mol% iron(II)-doped ZnO at 3.404 eV, 2.5 mol% iron(III)-doped ZnO at 3.406 eV and lastly undoped ZnO with the highest band gap energy of 3.408 eV.

Acknowledgement

The authors gratefully acknowledge CERVIE, UCSI University and research grant REIG-FETBE-2020/022 for the financial support.

Declaration of competing interests

The authors declare that they have no known competing financial interests or personal relationships that could have appeared to influence the work reported in this paper.

ORCID

Cheah Tian Chee Kingsly https://orcid.org/0000-0003-2659-9069
Jing Yao Sum https://orcid.org/0000-0001-9611-6304

References

[1] A. Ayele, D. Getachew, M. Kamaraj and A. Suresh, Phycoremediation of synthetic dyes: An effective and eco-Friendly algal technology for the dye abatement, Journal of Chemistry (2021) 9923643. https://doi.org/10.1155/2021/9923643.

[2] R. Islam, Water pollution due to textile industry, (2020). https://www.textiletoday.com.bd/water-pollution-due-textile-industry/ (accessed February 25, 2022).

[3] Z.Y. Velkova, G.K. Kirova, M.S. Stoytcheva and V.K. Gochev, Biosorption of Congo Red and methylene blue by pretreated waste streptomyces fradiae biomass - Equilibrium, kinetic and thermodynamic studies, Journal of the Serbian Chemical Society 83 (2018) 107–120. https://doi.org/10.2298/JSC170519093V.

[4] Y. Kayabaşı, Methylene blue and its importance in medicine, Demiroglu Science University Florence Nightingale Journal of Medicine 6 (2020) 136–145. https://doi.org/10.5606/fng.btd.2020.25035.

[5] A. Stelmach-Gołdyś, M. Zaborek-łyczba, J. Łyczba, B. Garus, M. Pasiarski, P. Mertowska, P. Małkowska, R. Hrynkiewicz, P. Niedźwiedzka-Rystwej and E. Grywalska, Physiology, Diagnosis and treatment of cardiac light chain amyloidosis, Journal of Clinical Medicine 11 (2022) 911. https://doi.org/10.3390/JCM11040911.

[6] I. Khan, K. Saeed, I. Zekker, B. Zhang, A.H. Hendi, A. Ahmad, S. Ahmad, N. Zada, H. Ahmad, L.A. Shah, T. Shah and I. Khan, Review on Methylene Blue: Its Properties, Uses, Toxicity and Photodegradation, Water (Basel). 14 (2022) 242. https://doi.org/10.3390/w14020242.

[7] N. Kaur, J. Kaushal, P. Mahajan and A.L. Srivastav, Design of hydroponic system for screening of ornamental plant species for removal of synthetic dyes using phytoremediation approach, (2022). https://doi.org/10.21203/rs.3.rs-1301660/v1.

[8] M.A. Abu-Dalo, S.A. Al-Rosan and B.A. Albiss, Photocatalytic degradation of methylene blue using polymeric membranes based on cellulose acetate impregnated with zno nanostructures, Polymers (Basel) 13(19) (2021) 3451. https://doi.org/10.3390/polym13193451.

[9] G. Ren, H. Han, Y. Wang, S. Liu, J. Zhao, X. Meng and Z. Li, Recent advances of photocatalytic application in water treatment: A review, Nanomaterials 11(7) (2021) 1804. https://doi.org/10.3390/nano11071804.

[10] C. Regmi, B. Joshi, S.K. Ray, G. Gyawali, R.P. Pandey, Understanding Mechanism of Photocatalytic Microbial Decontamination of Environmental Wastewater, Frontiers in Chemistry 6 (2018) 33. https://doi.org/10.3389/fchem.2018.00033.

[11] R. del Angel, J.C. Durán-Álvarez and R. Zanella, TiO2-Low band gap semiconductor heterostructures for water treatment using sunlight-driven photocatalysis, in: Titanium Dioxide - Material for a Sustainable Environment, InTech, 2018. https://doi.org/10.5772/intechopen.76501.

[12] N. Kamarulzaman, M.F. Kasim and R. Rusdi, Band gap narrowing and widening of ZnO nanostructures and doped materials, Nanoscale Research Letters 10 (2015) 346. https://doi.org/10.1186/s11671-015-1034-9.

[13] B. Albiss and M. Abu-Dalo, Photocatalytic degradation of methylene blue using zinc oxide nanorods grown on activated carbon fibers, Sustainability 13(9) (2021) 4729. https://doi.org/10.3390/su13094729.

[14] A.B. Mapossa, W. Mhike, J.L. Adalima and S. Tichapondwa, Removal of organic dyes from water and wastewater using magnetic ferrite-based titanium oxide and zinc oxide nanocomposites: A review, Catalysts 11(12) (2021) 1543. https://doi.org/10.3390/catal11121543.

[15] E. Cerrato, C. Gionco, I. Berruti, F. Sordello, P. Calza, M.C. Paganini, Rare earth ions doped ZnO: Synthesis, characterization and preliminary photoactivity assessment, Journal of Solid State Chemistry 264 (2018) 42-47. https://doi.org/10.1016/j.jssc.2018.05.001.

[16] M. Carofiglio, S. Barui, V. Cauda and M. Laurenti, Doped zinc oxide nanoparticles: Synthesis, characterization and potential use in nanomedicine, Applied Sciences 10(15) (2020) 5194. https://doi.org/10.3390/app10155194.

[17] A.B. Lavand and Y.S. Malghe, Synthesis, characterization and visible light photocatalytic activity of carbon and iron modified ZnO, Journal of King Saud University – Science 30 (2018) 65-74. https://doi.org/10.1016/J.JKSUS.2016.08.009.

[18] M.C. Paganini, A. Giorgini, N.P.F. Gonçalves, C. Gionco, A. Bianco Prevot and P. Calza, New insight into zinc oxide doped with iron and its exploitation to pollutants abatement, Catalysis Today 328 (2019) 230-234. https://doi.org/10.1016/j.cattod.2018.10.054.

[19] K.A. Isai and V.S. Shrivastava, Photocatalytic degradation of methylene blue using ZnO and 2%Fe–ZnO semiconductor nanomaterials synthesized by sol–gel method: a comparative study, SN Applied Sciences 1 (2019) 1247. https://doi.org/10.1007/s42452-019-1279-5.

[20] A. Razani, A.H. Abdullah, A. Fitrianto, N.A. Yusof, U.I. Gaya, Sol-gel synthesis of Fe2O3-doped TiO2 for optimized photocatalytic degradation of 2,4- dichlorophenoxyacetic acid, Oriental Journal of Chemistry 33 (2017) 1959–1968. https://doi.org/10.13005/OJC/330442.

[21] S.F. Mousavi, F. Davar, M.R. Loghman-Estarki, Controllable synthesis of ZnO nanoflowers by the modified sol–gel method, Journal of Materials Science: Materials in Electronics 27 (2016) 12985–12995. https://doi.org/10.1007/s10854-016-5437-x.

[22] A. Gnanaprakasam, V.M. Sivakumar and M. Thirumarimurugan, Influencing parameters in the photocatalytic degradation of organic effluent via Nanometal Oxide Catalyst: A review, Indian Journal of Materials Science 2015 (2015) 1–16. https://doi.org/10.1155/2015/601827.

[23] R.P. Pal Singh, I.S. Hudiara and S.B. Rana, Effect of calcination temperature on the structural, optical and magnetic properties of pure and Fe-doped ZnO nanoparticles, Materials Science- Poland 34 (2016) 451–459. https://doi.org/10.1515/msp-2016-0059.

[24] S. Babel, H. Sudrajat and A.A. Abraham, Manganese-and iron-doped zinc oxide for photocatalytic degradation of recalcitrant dyes, Thammasat International Journal of Science and Technology 21(4) (2016) 33-43. https://doi.org/10.14456/tijsat.2016.28.

[25] J.Z. Lian, C.T. Tsai, S.H. Chang, N.H. Lin and Y.H. Hsieh, Iron waste as an effective depend on TiO_2 for photocatalytic degradation of dye waste water, Optik 140 (2017) 197–204. https://doi.org/10.1016/J.IJLEO.2017.04.023.

[26] V.M. Thanh, N.T. Huong, D.T. Nam, N.D.T. Dung, le Van Thu and M.T. Nguyen-Le, Synthesis of ternary Fe_3O_4/ZnO/chitosan magnetic nanoparticles via an ultrasound-assisted coprecipitation process for antibacterial applications, Journal of Nanomaterials 2020 (2020) 8875471. https://doi.org/10.1155/2020/8875471.

[27] S. Roy, M.P. Ghosh, S. Mukherjee and P. Ghosh, Introducing the magnetic properties in Fe doped ZnO nanoparticles for spintronics application, (2021). https://doi.org/10.21203/rs.3.rs-180286/v1.

[28] P. Makuła, M. Pacia and W. Macyk, How to correctly determine the band gap energy of modified semiconductor photocatalysts based on UV-Vis spectra, Journal of Physical Chemistry Letters 9 (2018) 6814–6817. https://doi.org/10.1021/acs.jpclett.8b02892.

[29] G. Yentür and M. Dükkancı, Synergistic effect of sonication on photocatalytic oxidation of pharmaceutical drug carbamazepine, Ultrasonic Sonochemistry 78 (2021) 105749. https://doi.org/10.1016/j.ultsonch.2021.105749.

[30] N.N. Yunus, F. Hamzah, M.S. So'Aib and J. Krishnan, Effect of catalyst loading on photocatalytic degradation of phenol by using N, S Co-doped TiO_2, IOP Conference Series: Materials Science and Engineering 206 (2016) 012092. https://doi.org/10.1088/1757-899X/206/1/012092.

[31] H. Yang, J. Fan, C. Zhou, R. Luo, H. Liu, Y. Wan, J. Zhang, J. Chen, G. Wang, R. Wang and C. Jiang, Co_3O_4@CdS hollow spheres derived from ZIF-67 with a high phenol and dye photodegradation activity, ACS Omega 5 (2020) 17160–17169. https://doi.org/10.1021/acsomega.0c01131.

[32] T. Munir, M. Latif, A. Mahmood, A. Malik and F. Shafiq, Influence of IP-injected ZnO-nanoparticles in Catla catla fish: hematological and serological profile, Naunyn-Schmiedeberg's Archives of Pharmacology 393 (2020) 2453–2461. https://doi.org/10.1007/s00210-020-01955-6.

[33] P.J. Lu, W.E. Fu, S.C. Huang, C.Y. Lin, M.L. Ho, Y.P. Chen and H.F. Cheng, Methodology for sample preparation and size measurement of commercial ZnO nanoparticles, Journal of Food and Drug Analysis 26 (2018) 628–636. https://doi.org/10.1016/j.jfda.2017.07.004.

[34] H. Sutanto, I. Alkian, M. Mukholit, A.A. Nugraha, E. Hidayanto, I. Marhaendrajaya and P. Priyono, Analysis of Fe-doped ZnO thin films for degradation of rhodamine b, methylene blue, and Escherichia coli under visible light, Materials Research Express 8 (2021) 116402. https://doi.org/10.1088/2053-1591/ac33fe.

[35] K.V.A. Kumar, B. Lakshminarayana, T. Vinodkumar and C. Subrahmanyam, Cu-ZnO for visible light induced mineralization of Bisphenol-A: Impact of Cu ion doping, Journal of Environmental Chemical Engineering 7 (2019) 103057. https://doi.org/10.1016/j.jece.2019.103057.

[36] A. Kumar, A review on the factors affecting the photocatalytic degradation of hazardous materials, Material Science & Engineering International Journal 1(3) (2017) 106-114. https://doi.org/10.15406/mseij.2017.01.00018.

[37] M. Boumediene, H. Benaïssa, B. George, S. Molina and A. Merlin, Effects of pH and ionic strength on methylene blue removal from synthetic aqueous solutions by sorption onto orange peel and desorption study, Journal of Materials and Environmental Science 9 (2018) 1700–1711. https://doi.org/10.26872/jmes.2018.9.6.190.

[38] N. Bel, H. Mohamed, S. Ouni, M. Bouzid, M. Bouzidi and A. Bonilla-Petriciolet, Adsorption and photocatalytic degradation of an industrial azo dye using colloidal semiconductor nanocrystals, (2022). https://doi.org/10.21203/rs.3.rs-1057236/v2.

[39] S.R. Sowmya, G.M. Madhu and M. Hashir, Studies on Nano-Engineered TiO2 Photo Catalyst for Effective Degradation of Dye, IOP Conference Series: Materials Science and Engineering 310 (2018) 012026. https://doi.org/10.1088/1757-899X/310/1/012026.

[40] N.B. Swan and M.A.A. Zaini, Adsorption of Malachite green and congo red dyes from water: Recent progress and future outlook, Ecological Chemistry and Engineering S 26 (2019) 119–132. https://doi.org/10.1515/eces-2019-0009.

[41] H.R. Sousa, L.S. Silva, P.A.A. Sousa, R.R.M. Sousa, M.G. Fonseca, J.A. Osajima and E.C. Silva-Filho, Evaluation of methylene blue removal by plasma activated palygorskites, Journal of Materials Research and Technology 8 (2019) 5432–5442. https://doi.org/10.1016/j.jmrt.2019.09.011 .

[42] K. Litefti, M.S. Freire, M. Stitou and J. González-Álvarez, Adsorption of an anionic dye (Congo red) from aqueous solutions by pine bark, Scientific Report 9 (2019) 16530. https://doi.org/10.1038/s41598-019-53046-z.